Thermoresponsive gel embedding extracellular vesicles from adipose stromal cells improves the healing of colonic anastomoses following irradiation in rats

Hadrien Alric, Noelle Mathieu, Anna Sebbagh, Guillaume Peré, Christelle Demarquay, André Cronemberger, Arthur Berger, Benjamin Marcel, Claire Wilhelm, Florence Gazeau, et al.

communications biology

Article

https://doi.org/10.1038/s42003-024-07364-2

Thermoresponsive gel embedding extracellular vesicles from adipose stromal cells improves the healing of colonic anastomoses following irradiation in rats

Hadrien Alric[1,2,11] ✉, Noëlle Mathieu[3,11], Anna Sebbagh[4], Guillaume Peré[1,5], Christelle Demarquay[3], André Cronemberger[4], Arthur Berger[1,6], Benjamin Marcel[4], Claire Wilhelm[7], Florence Gazeau[4], Antoine Mariani[1,8], Mehdi Karoui[1,8], Olivier Clément[1,9], Irami Araujo-Filho[10], Amanda K. A. Silva[4,11] & Gabriel Rahmi[1,2,11]

Anastomotic leak occurrence is a severe complication after colorectal surgery. Considering the difficulty of treating these leaks and their impact on patient care, there is a strong need for an efficient prevention strategy. We evaluated a combination of extracellular vesicles (EVs) from rat adipose-derived stromal cells with a thermoresponsive gel, Pluronic® F127 (PF-127) to prevent anastomotic leaks. The pro-regenerative and immunomodulatory potencies of EVs are assessed in vitro. In vivo efficacy are assessed in rat with a colonic anastomosis model after irradiation. Endoscopic, anatomical and histological data show a consistent effect of EVs + gel on the healing of colonic anastomosis. These results are illustrated by a smaller anastomotic ulcer size, less fibrosis and less inflammatory infiltrations in the EVs + gel group. This multi-modal investigation is the first to point-out the translational potential of EVs combined with PF-127 for the healing of high-risk colorectal anastomosis.

The incidence of rectal cancer worldwide is 732,210 per year[1]. Neoadjuvant chemoradiotherapy supplemented by surgery with a low colorectal or colo-anal anastomosis is recommended in locally advanced disease[2]. Despite years of research, the incidence of anastomotic leak after rectal surgery remains high, ranging from 3 to 21%[3,4] and is associated with increased morbidity, mortality, and cancer recurrence[5]. Furthermore, anastomotic leaks are associated with an increased healthcare burden due to the higher costs of management and the use of resources for remedial care[6]. It is known that anastomotic leak etiology is multifactorial. Excluding technical failures, there is accumulating evidence pointing at anastomotic leak as the result of a complex, dynamic interplay of several factors and biological processes[7–9]. This includes host genetics, gut microbiome, inflammation, and the immune system[10]. The occurrence of anastomotic leak might also be linked to TNM stage and patient nutritional status[11], along with treatment-related factors. Indeed, while preoperative chemoradiotherapy for rectal cancer improves local

[1]Laboratoire de Recherche en Imagerie du Vivant, PARCC, INSERM U970, Université Paris Cité, Paris, France. [2]Service d'Hépato-Gastro-Entérologie et Endoscopies Digestives, Hôpital Européen Georges Pompidou, APHP.Centre—Université Paris Cité, Paris, France. [3]Laboratoire de Radiobiologie des Expositions Médicales, Institut de Radioprotection et de Sureté Nucléaire, Fontenay-Aux-Roses, France. [4]Laboratoire Matière et Systèmes Complexes, CNRS, UMR 7057, Université Paris Cité, Paris, France. [5]Service de Chirurgie Digestive, Centre-Hospitalo-Universitaire Toulouse-Rangueil, Toulouse, France. [6]Service d'Hépato-Gastroentérologie et Oncologie Digestive, Centre-Hospitalo-Universitaire Bordeaux, Bordeaux, France. [7]Laboratoire PhysicoChimie Curie, Institut Curie, PSL Research University—Sorbonne Université—CNRS, Paris, France. [8]Service de Chirurgie Digestive, Hôpital Européen Georges Pompidou, Assistance Publique Hôpitaux de Paris, Paris, France. [9]Service d'Imagerie, Hôpital Européen Georges Pompidou, Assistance Publique Hôpitaux de Paris, Paris, France. [10]Department of Surgery, Federal University of Rio Grande do Norte. Institute of Teaching, Research, and Innovation, Liga Contra o Cancer, Natal, Brazil. [11]These authors contributed equally: Hadrien Alric, Noëlle Mathieu, Amanda K. A. Silva, Gabriel Rahmi. ✉e-mail: Hadrien.alric@aphp.fr

disease control, it can induce inadequate anastomotic healing and has also been described as a risk factor for anastomotic leak[12,13].

Regenerative medicine has provided new therapeutic options for preventing anastomotic leak. Thus, various preclinical studies have demonstrated the effectiveness of mesenchymal stromal cells (MSCs) in the prevention of anastomotic leak[14–17]. However, other studies seem to challenge the hypothesis that MSCs contribute directly to tissue regeneration. On the one hand, it was shown that an inflammatory environment at the injury site is strongly deleterious to MSCs survival[18]. On the other hand, the therapeutic effect of MSCs seems to occur in a too short period to be attributed solely to their direct differentiation into functional cells[19]. These results suggest that the effectiveness of MSCs is rather mediated by a paracrine effect[20]. Thus, the investigation of extracellular vesicles (EVs) derived from these MSCs participating in their paracrine effect seems to represent an interesting alternative. EVs are lipid bilayer vesicles with a size range of 50–2000 nm that are released by cells into the extracellular spaces. They are considered cargo delivery vesicles because they harbor nucleic acids, proteins, lipids, and metabolites that reflect their cellular origin[21,22]. They have the advantage of being more easily stored and administered and do not present any risk of proliferation or uncontrolled differentiation[19,23]. In addition, previous studies showed the beneficial effect of EVs in the therapy of heart, kidney, liver, brain, and skin injuries[24–28].

Administration of EVs could be challenging because systemically administered EVs have a short half-life and rapid internalization by the liver and spleen[29]. This underlines the importance of local rather than systemic administration to improve retention of EVs at the site of interest[30]. In this context, the combination to a thermoresponsive hydrogel, for instance Pluronic F-127 (PF-127),may be of interest. Due to its thermoresponsive properties, it features a transition temperature below which it is injectable and above which its viscosity is high enough to increase the residence time in the site of interest[31]. Thus, PF-127 is easily injectable through a catheter in the liquid form gelling at 37 °C expecting to increase the contact time of and the embedded EV in the tissue. In two preclinical studies, our team used the association of PF-127 gel and EVs in a porcine model of esophageal fistula and in a rat model of colo-cutaneous fistula[32,33]. We were able to demonstrate that the gel had the capacity to retain EVs at the site of interest inducing a healing effect.

The objective of this preclinical study was to evaluate the feasibility and efficacy of allogeneic EVs derived from rat adipose-derived stromal cells (ADSCs) combined or not to PF-127 gel to improve the healing of high-risk colonic anastomoses in an irradiated colon rat model.

Results

ADSC phenotype and differentiation

Cells isolated from adipose tissue showed a homogeneous spindle-shaped morphology. The capacity to form colony-forming units was evaluated: there were 41.17 (±7.25) for 1000 cells seeded in 25 cm^2. The phenotype of the cells was analyzed for stromal characteristics by flow cytometry at passage 0 (Fig. 1a). The cells expressed high levels of CD90, CD73, and CD29, and were negative for hematopoietic markers, which was consistent with an ADSC phenotype. On average, the cells expressed CD90 at 99.9% (±0.14%), CD73 at 99.9% (±0.14%), CD29 at 100.0% (±0.08%), CD34 at 0.7% (±0.01%) and CD45 at 0.5% (±0.01%).

Allogeneic ADSC EVs produced by turbulence featured classical EV size and markers according to nanoparticle tracking analysis and nano-flow cytometry

Using the method described below (Methods, "*EVs production*"), we were able to obtain $1.26.10^{12}$ EVs in a bioreactor of 1 L. The mean size and mode were 126.1 nm and 86.7 respectively, consistent with typical EV size range (Fig. 1b). For this sample, 90% of particles were smaller than 182.1 nm, 50% of particles were smaller than 110.9 nm, and 10% of particles were smaller than 81.0 nm.

The expression of EV markers CD63, CD81, and CD9 was verified by nano-flow cytometry (Supplementary Fig. S1). 8.7 ± 3.9% of all detected particles were positive for CD9; 14.9 ± 4.1% of all detected particles were positive for CD81; and 19.7 ± 4.7% of all detected particles were positive for CD63.

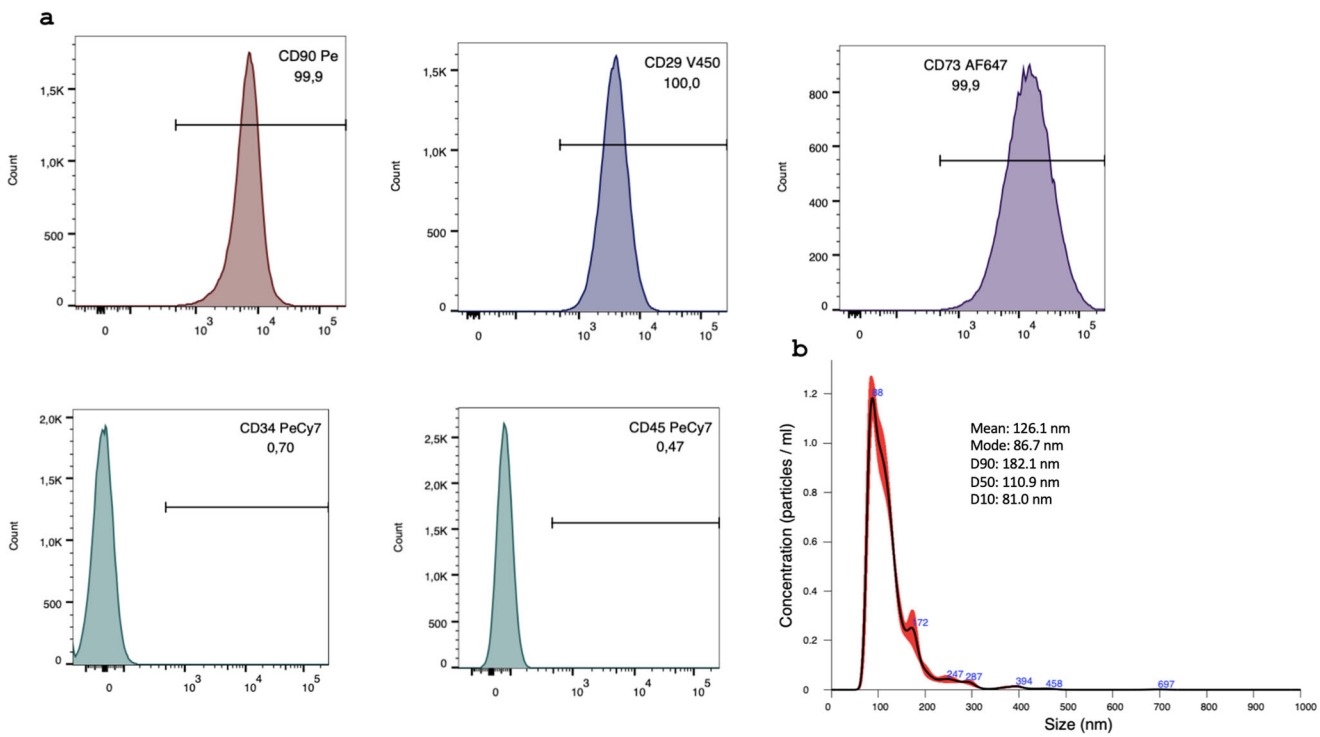

Fig. 1 | Characterization of ADSC and EVs. The phenotype of amplified ADSC analyzed by flow cytometry before EVs production. Histograms representing the percentage of CD90, CD29, and CD73 mesenchymal markers, and CD34 and CD45 hematopoietic markers (**a**). After production, EVs concentration, mean, and mode were obtained by nanoparticle tracking analysis (**b**).

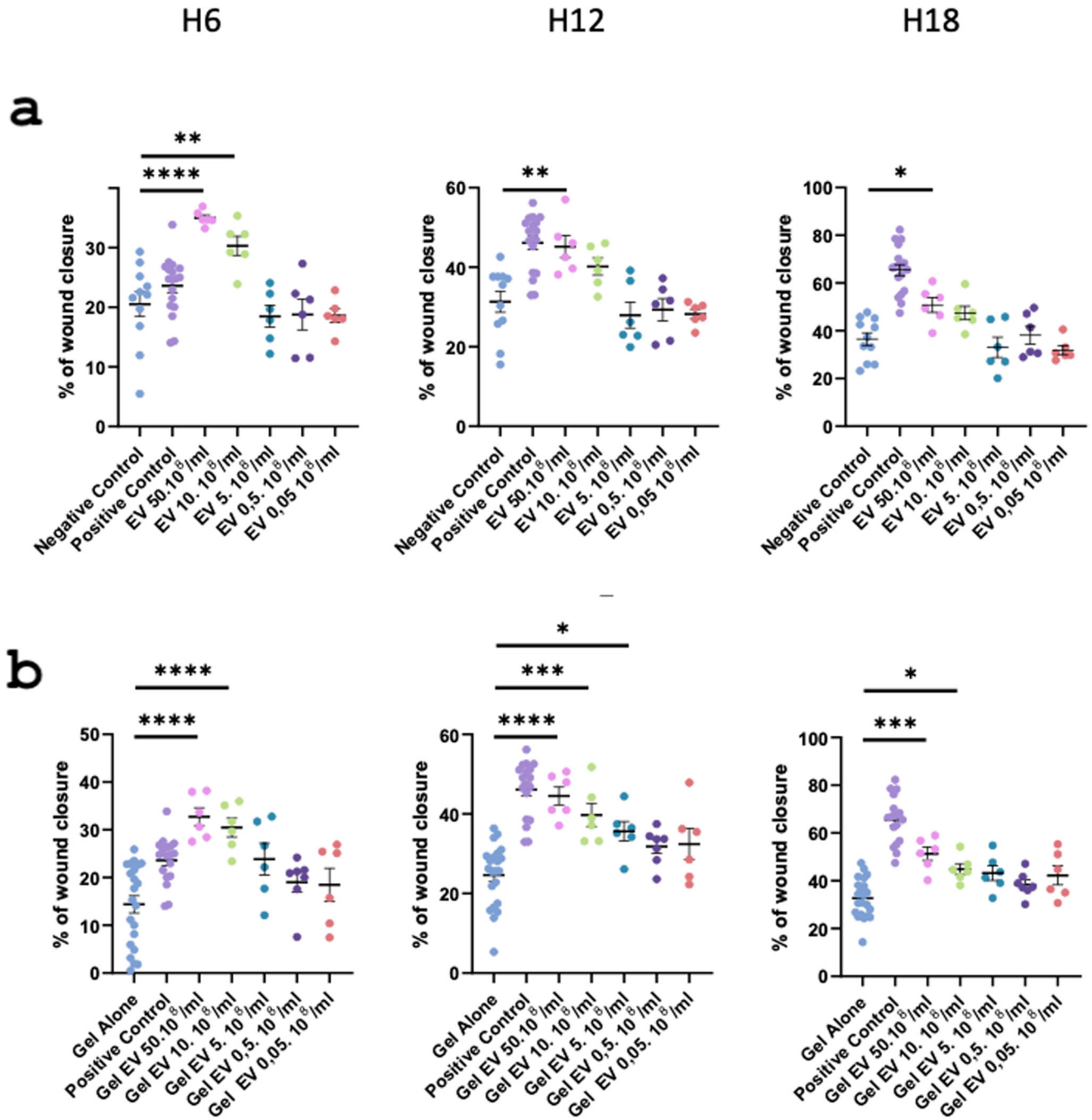

Fig. 2 | In vitro pro-angiogenic effect of EVs, assessed by scratch tests in HUVEC cells. a Percentage of wound closure with increasing doses of EVs at 6 h, 12 h, and 18 h. Results are shown as the mean ± standard deviation with individual values ($n = 12$ biological replicates from 2 independent experiments). **b** Percentage of wound closure with increasing doses of gel-encapsulated EVs at 6 h, 12 h and 18 h. Results are shown as the mean ± standard deviation with individual values (**n** = 12 biological replicates from 2 independent experiments).

The integrity of EVs suspended in Phosphate-Buffered Saline (PBS) and EVs embedded in PF-127 was verified through Transmission Electron Microscopy (TEM) (Supplementary Fig. S2).

Allogeneic ADSC EVs induce in vitro pro-angiogenic effects as assessed through scratch tests on human umbilical vein endothelial cells

To evaluate the pro-angiogenic potential of EVs in vitro, we performed scratch tests on cells of the human umbilical vein endothelial cells (HUVEC) cell line, treated or not with EVs. We compared cell wound closure at three different time-points (6 h, 12 h and 18 h) as a function of EV concentration (50.10^8 EVs/mL, 10.10^8 EVs/mL, 5.10^8 EVs/mL, 0.5 10^8EVs/mL, $0.05.10^8$ EVs/mL).

We first studied the effect of increasing EV concentrations (Fig. 2a). After 6 h of incubation, the 50.10^8 EVs/mL concentration provided better wound closure compared to the negative and positive control ($p < 0.001$ and $p < 0.01$ respectively). There was no difference for lower concentrations compared to the negative control. After 12 and 18 h, the percentage of wound closure was statistically higher in the 50.10^8 EVs/mL group compared to the negative control alone ($p < 0.01$ and $p < 0.05$ respectively).

In a second step, we evaluated the effect of increasing the concentration of EVs embedded in PF-127 (Fig. 2b). After 6 h of incubation, the 50.10^8

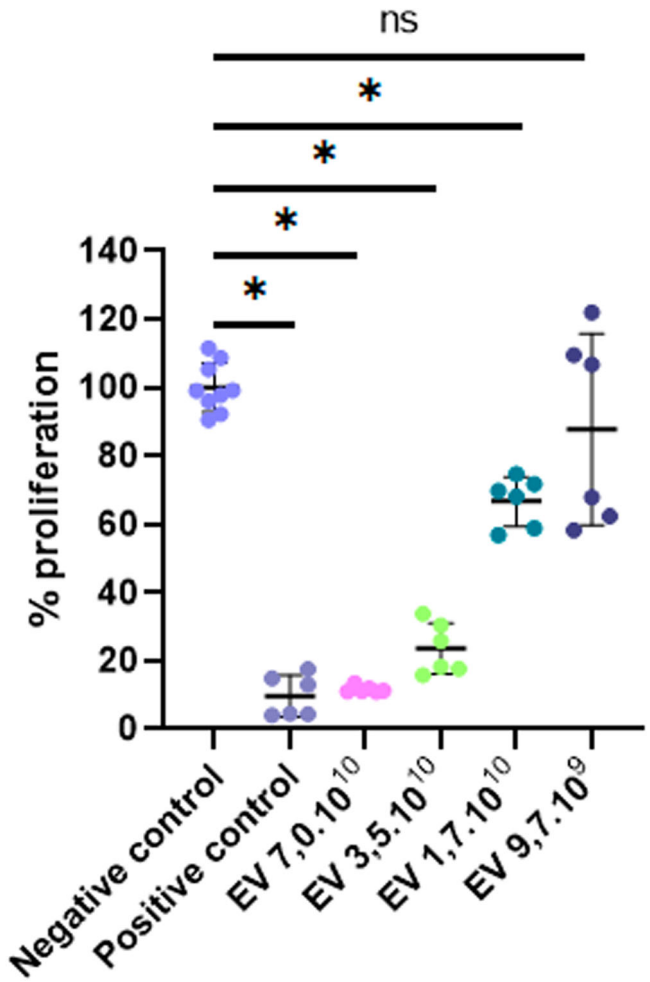

Fig. 3 | In vitro immunomodulatory potential of EVs, assessed by mixed lymphocyte reaction. Lymphocytes from SD /CD and Wistar rat strains were mixed, stimulated for 48 h with PHA-M and ConA, then treated with rat ADSC EVs at a dose ranging from 0 (negative control) to $7.0.10^{10}$ particles per well. Lymphocyte proliferation rates were assessed at 24 h and normalized to the proliferation rate observed in the negative control group. Data are shown as the mean ± SD with individual values (6 biological replicates from 2 independent experiments per group).

EVs/mL and 10.10^8 EVs/mL concentrations provided better wound closure compared to the negative control ($p < 0.001$ and $p < 0.001$ respectively). After 12 h, the 50.10^8 EVs/mL, 10.10^8 EVs/mL, and 5.10^8 EVs/mL concentrations exhibited significantly improved wound closure compared to the negative control ($p < 0.001$, $p < 0.01$, and $p = 0.05$, respectively). After 18 h of incubation, the 50.10^8EVs/mL and 10.10^8 EVs/mL concentrations provided better wound closure compared to the negative control ($p < 0.001$ and $p < 0.05$ respectively).

Allogeneic ADSC EVs mediate immunomodulatory effects as assessed through mixed lymphocyte reaction

To evaluate the immunomodulatory potential of EVs, we performed two-way Mixed Lymphocyte Reaction (MLR) on PHA-M and ConA-stimulated lymphocytes from SD/CD and Wistar rats (Fig. 3). ADSCs were used as a positive control. At 24 h, the mean normalized lymphocyte proliferation rate reached 100.0 ± 7.2% in the negative control group compared to 9.7 ± 6.1% in the positive control group ($p = 0.018$). Treatment with rat ADSC EVs significantly decreased lymphocyte proliferation compared to the negative control group, reaching respectively 11.6 ± 1.0% ($p = 0.018$), 23.6 ± 7.5% ($p = 0.018$), 66.6 ± 7.2% ($p = 0.018$) and at doses of respectively $7.0.10^{10}$, $3.5.10^{10}$, $1.7.10^{10}$ particles per well. Treatment with rat ADSC EVs at the lowest dose tested ($8.7.10^9$ particles per well) failed to decrease lymphocyte proliferation compared to the negative control (87.8 ± 28.0%, $p = 0.999$); and lymphocyte proliferation rates were significantly lower after treatment with either of the two highest EV doses compared to all lower doses ($p = 0.046$ in all cases), hinting at a potential dose-dependent immunomodulatory effect of rat ADSC EVs.

Results of surgical intervention

Surgery was performed 3 weeks after colorectal irradiation, during which the treatment of interest was applied: control, PF-127 alone, EVs alone or PF-F127 containing EVs (Fig. 4). The average operative time was 49.6 (±1.1) min. The mean weight before surgery was 497.0 (±35.6) g. At the end of the follow-up, the mean weight was 548.0 (±68.6) g. Of the 40 rats that underwent surgery, 6 died before completing the study. In the control group, one rat died on the 4th post-operative day from stercoral peritonitis; another rat was euthanized after 4 weeks of post-operative follow-up due to major weight loss and behavioral alterations, a small bowel leak was found at autopsy. In the group receiving PF-127 alone, one rat was euthanized after 4 weeks of post-operative follow-up, a small bowel leak was found; another rat died intra-anesthetically during surgical procedure. In the group receiving EVs alone, one rat died at 3 weeks of post-operative follow-up, autopsy could not be performed. In the EVs + gel group, one rat was euthanized the day after surgery due to evisceration.

Allogeneic ADSC EVs combined with PF-127 gel decrease colonic anastomosis inflammation

At 8 weeks after the end of colorectal irradiation, a colonoscopy was performed to evaluate the healing of the anastomosis before euthanasia. Representative images are shown for each group in Fig. 5a. The severity of residual lesions at the level of colonic anastomoses was evaluated through the measurement of an ENDOSCORE, which graded ulcer severity, bleeding and anastomotic strictures (Fig. 5b, c). The ENDOSCORE was significantly lower in the EVs + gel group compared to the control group (2.4 ± 1.1 vs 3.8 ± 1.1; $p < 0.05$). A similar trend to a decrease of the ENDOSCORE compared to the negative control was observed in the EVs group, though it failed to reach statistical significance (2.9 ± 1.5 versus 3.9 ± 1.1; NS). Treatment with the gel alone did not seem to decrease the ENDOSCORE compared to the control group (3.9 ± 1.5 versus 3.8 ± 1.1; NS).

Immediately after colonoscopy, the rats were sacrificed and an autopsy was performed to assess the presence of peritoneal adhesions (Fig. 5d). The Zuhlke score, describing the strength of peritoneal adhesions, was significantly lower in the EVs (1.1 ± 0.2 versus 2.2 ± 0.4; $p < 0.05$) and EVs + gel groups compared to the control group (1.2 ± 0.3 versus 2.2 ± 0.4; $p < 0.05$) (Fig. 5e). There was also a trend towards a lower number of abdominal structures adhering to the anastomosis in both EV-treated groups compared to the control, though it failed to reach statistical significance (Fig. 5f). There was no difference between the gel group and the control group.

Rats treated with ADSC EVs in the PF-127 gel demonstrated histologic evidence of improvement in both inflammation and fibrosis at the anastomotic site

The rats were sacrificed 8 weeks post irradiation and, just after the autopsy, the colonic specimens were extracted for histological analyses. After HES staining, we assessed the healing of the anastomosis by measuring the sizes of the colonic scars (Fig. 6a, b). We observed that the ulcerated anastomotic area was significantly smaller after treatment with EVs and gel-embedded EVs compared to control group (respectively 715.8 ± 103.8 µm and 683.5 ± 128.0 µm compared to 1912 ± 129.5 µm, with $p < 0.01$ in both cases).

We then assessed the percentage of the anastomotic zone corresponding to fibrosis after staining by SR and analysis by our FIBER software (Fig. 6c, d). Thus, the group treated with gel-embedded EVs had a lower area of fibrosis compared to the control group (46.6 ± 2.9% vs 54.7 ± 2.7%

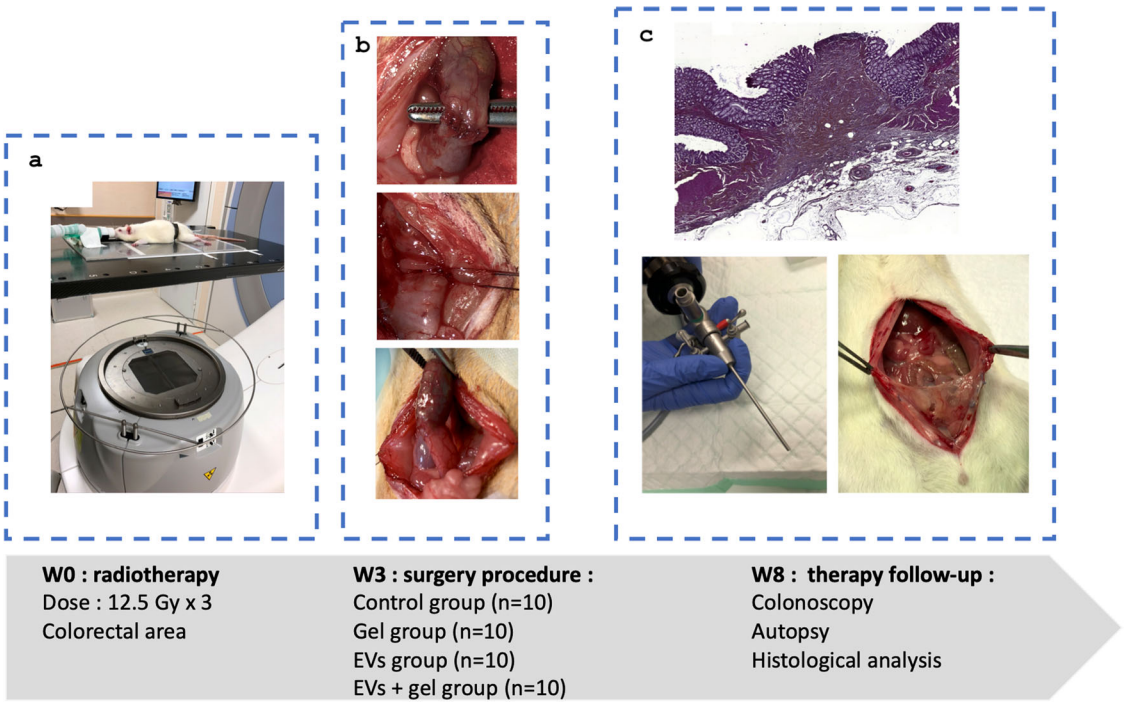

Fig. 4 | Design of the in vivo experimental protocol. A 12.5 Gy dose was delivered three times in 1 week through a 2 × 3 cm window centered on the colorectal region using a medical accelerator (**a**). Surgery was performed 3 weeks later with a low colo-colic anastomosis during which the treatment was applied: control (surgery procedure with administration of PBS), PF-127 alone, EVs alone, or PF-127 containing EVs (**b**). Eight weeks after the end of the irradiation, colo-colic anastomoses were evaluated by colonoscopy. Immediately after colonoscopy, the rats were sacrificed, and an autopsy was performed. The colonic anastomosis was then extracted for histological analysis (**c**).

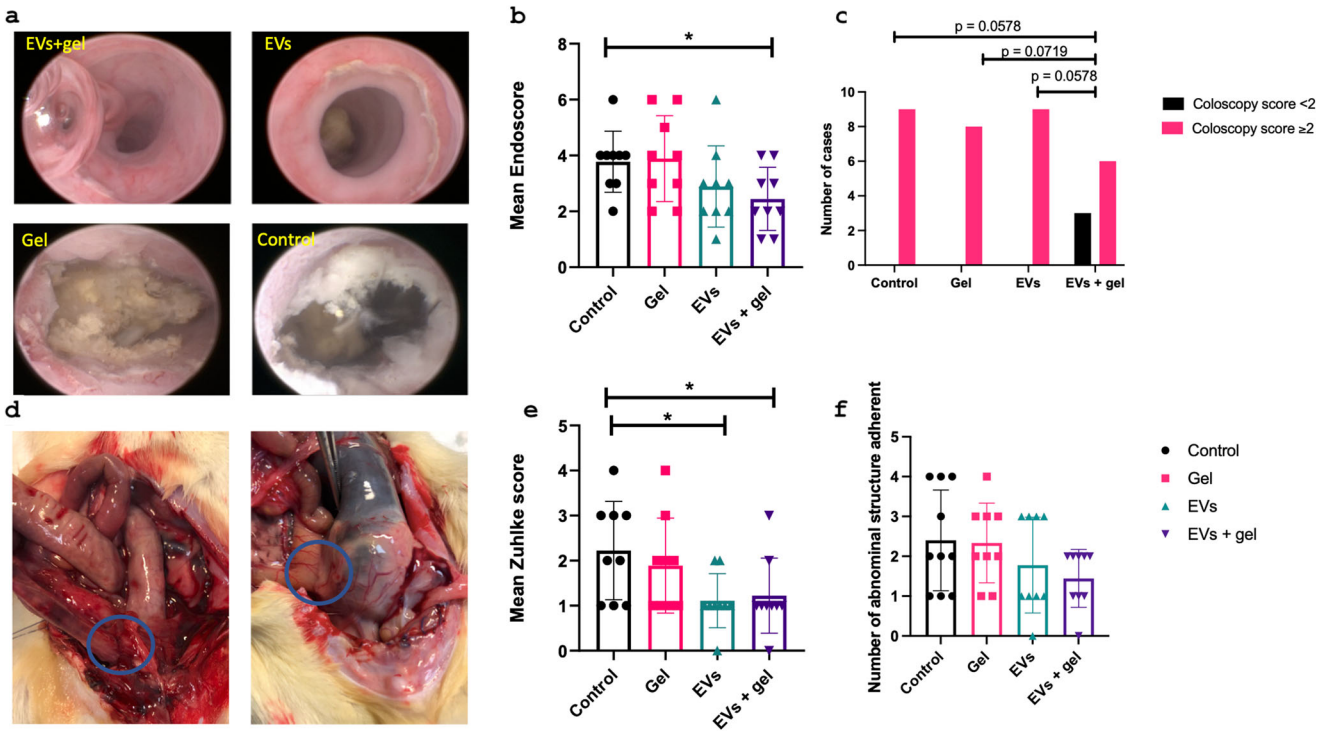

Fig. 5 | Clinical evaluation at W8. Representative colonoscopy pictures of the different group (**a**): the presence of anastomotic ulceration and its characterization was noted according to its severity (1: no ulcer, 2: superficial ulcer, 3: deep ulcer, 4: deep circumferential ulcer). Bleeding or stenosis of the anastomosis was also reported and combined in an ENDOSCORE (**b** and **c**). Pictures of colo-colic anastomosis during the autopsy (**d**). The blue circles highlight two entero-anastomotic fistulas. Graph representing the peritoneal adhesions by the Zuhlke score (**e**) and the number of structures adherent to the anastomosis (seminal vesicles, bladder, small bowel) (**f**).

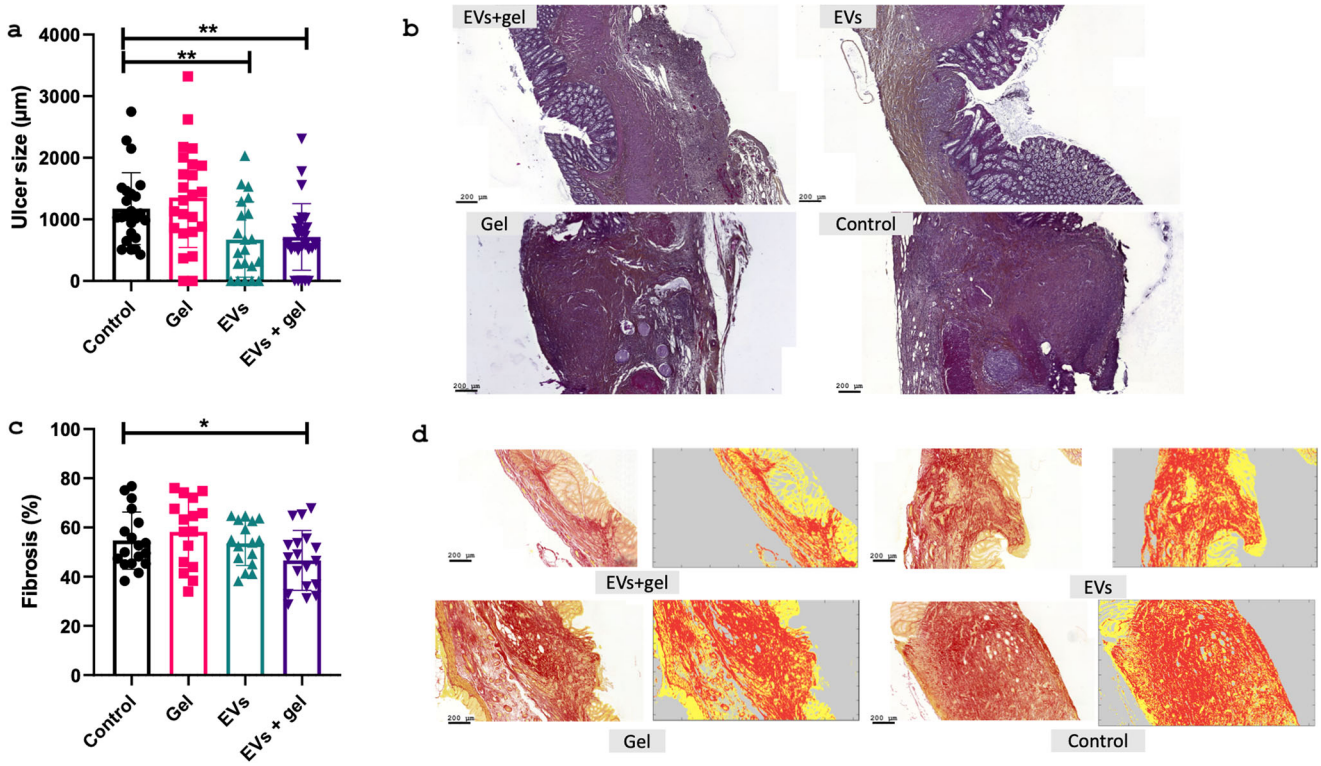

Fig. 6 | Histological analysis of the anastomosis. a graph representing the measurement of ulcer size at the anastomosis site (±SD). Two series of slides were analyzed in 8 rats of the control and gel groups. Nine rats of the EVs and EVs+gel groups were analyzed. **b** representative picture of HES slides at the colo-colic anastomosis level in the different groups (scale bar = 200µm). **c** graph representing the percentage (±SD) of fibrosis at the anastomosis level using the FIBER-ML program (scale bar = 200 µm). Two series of slides were analyzed in 8 rats of the control and gel groups. Nine rats of the EVs and EVs+gel groups were analyzed. **d** representative picture of RS slides and after the use of FIBER-ML program at the colo-colic anastomosis level (scale bar = 200 µm).

$p < 0.05$). No differences were found between the other groups compared to the control.

We then analyzed the anastomotic area using immunohistochemical staining with myeloperoxidase (MPO) and CD68 (Fig. 7). We observed that the MPO-marked polymorphonuclear neutrophils (PMN) infiltrate was significantly lower in the gel-embedded EVs group and in the EVs group compared to the control group (with respectively 103.0/mm^2 ± 47.7 versus 230.0/mm^2 ± 73.9, $p < 0.01$; and 71.0/mm^2 ± 62.6 versus 230.0/mm^2 ± 73.9 $p < 0.01$, Fig. 7a, b). In contrast, the CD68-marked macrophagic infiltrate was not different between the treatment and control groups (Fig. 7c, d).

Discussion

To the best of our knowledge, this is the first time that ADSC derived-EVs embedded in a thermoresponsive gel are investigated for the therapy of a high-risk digestive anastomosis.

Anastomotic leaks are a frequent and potentially severe complication in colorectal surgery. An appropriate surgical technique including gentle handling of the bowel, avoidance of pressure at anastomosis, and suture of well-vascularized tissue seem to be critical for a successful colorectal anastomosis[34]. In addition to these technical parameters, it has recently been suggested that anastomotic leak may result from a complex and dynamic interplay of biological factors[7] such as the initial inflammatory response, collagen deposition, wound remodeling[35], and anastomotic perfusion notably post radiotherapy[36]. In this study, we used a high-risk colorectal anastomosis model in rats irradiated in the colorectal region, which was previously described in other works of our team[14,37].

It seemed relevant to us to investigate EVs derived from ADSCs for the healing of colonic anastomoses, considering that we have already demonstrated a therapeutic effect of these cells in this preclinical model[14,37]. In these studies, the local and systemic use of ADSCs allowed better healing of colonic anastomoses in association with improved vascularization and the presence of M2-type macrophages with anti-inflammatory characteristics. Thus, as it has been proposed in the literature that the beneficial effects of some cell therapies may derive more from secreted EVs, we investigated ADSC EVs rather than the cells themselves[38]. ADSC-EVs were produced by an innovative high-yield method in bioreactors[39]. Our team has shown that this method may enable up to a 10-fold increase in EV yield and a 10-fold faster production compared to state-of-the-art method (starvation approach in 48 h), with EVs featuring equivalent potency in vitro[40]. This high-yield turbulence approach[41] enabled us to produce 1.26.10^{12} EVs in a bioreactor of 1 L. In this study, we produced EVs with an average size of 126 nm, which expressed the tetraspanins CD9, CD63, and CD81; three markers which are characteristically enriched in EVs. Our group had previously provided evidence on the therapeutic effects of murine MSC EVs or porcine ADSC EVs obtained by the turbulence method in a rat model of colo-cutaneous fistula and a pig model of esophageal stricture, respectively[32,33,41].

Here, EVs were embedded in PF-127 thermoresponsive hydrogel for a local application at the level of anastomosis during surgery. We chose PF-127 gel at 20% for its thermoresponsive ability to be applied as a liquid at <20 °C undergoing gel transition >20 °C upon contact with the surgical anastomotic area at body temperature[42]. We have shown in another study, using [^{89}Zn] labeled EVs, that the use of this gel allowed a better retention of EVs on the site of interest compared to saline solution[33]. The combination of EVs and PF-127 was previously analyzed by our team via rheological analyses and NTA[32], showing that the dispersion of EVs into PF-127 did not change its thermoresponsive properties and seemed to have a minor impact on EVs integrity. We also evidenced that the aqueous dilution of the gel to a concentration below 13% induced the transition from gel to solution releasing EVs, as demonstrated by NTA[32]. On the basis of these data, we chose a gel concentration of 20% to allow for a gradual delivery of EVs at the anastomosis through progressive dilution with digestive secretions.

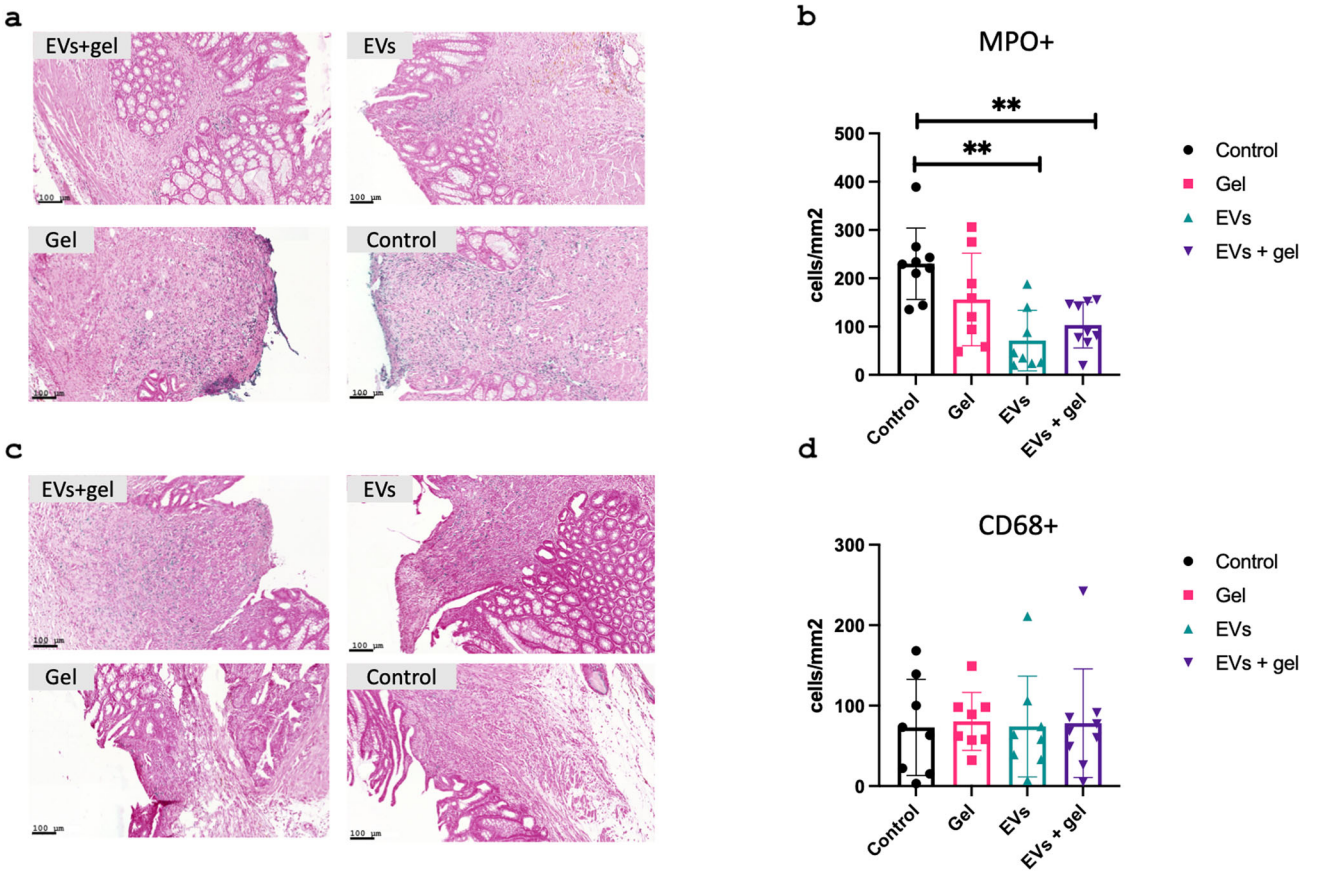

Fig. 7 | Immunohistochemical analysis of the anastomosis. a representative picture of MPO immunostaining at the colo-colic anastomosis level in the different groups. Blue coloration corresponds to PMN cells and pink coloration corresponds to counter-colored tissue (scale bar = 100 µm). **b** graph representing the number of MPO positive cells per surface unit (±SD). **c**: representative of CD68 immunostaining at the colo-colic anastomosis level in the different groups. Blue coloration corresponds to macrophages and pink coloration corresponds to counter-colored tissue (scale bar = 100µm). **d** graph representing the number of CD68 positive cells per surface unit (±SD).

In the present study, we confirmed by TEM that EVs appear to maintain their integrity even when embedded in PF-127. We investigated EV in vitro immunomodulatory potential by two-ways MLR, evidencing a dose-dependent decrease of lymphocyte proliferation with EV treatment. We evaluated EV in vitro pro-angiogenic potential using scratch tests on endothelial cells of the HUVEC cell line. We observed a statistically higher percentage of wound closure in the 50.10^8 EVs/mL group compared to the negative control at 6 h, 12 h, and 18 h, both when EVs were administered in the PF-127 hydrogel and when they were administered in saline. These results are in line with many other studies hinting at potential immunomodulatory[43–46] or pro-angiogenic effects of MSC-derived EVs[47,48].

Interestingly, our preliminary in vitro data would seem to suggest that the effect of EVs might be more sustained when they are embedded in the PF-127 hydrogel. Indeed, in the scratch tests, a statistically higher wound closure was observed for the concentration 10.10^8 EVs/mL at 12 h and 18 h and for the concentration of 5.10^8 EVs/mL at 12 h compared to the negative control, but only when EVs were combined to the hydrogel. These results might suggest that the use of PF-127 hydrogel would allow a slower and longer lasting diffusion of EVs over the area of interest than a direct application in saline solution. These data also indicate that EVs preserve their therapeutic effect after being released from the PF-127 hydrogel. This is of interest considering the development of a strategy for local and sustained therapeutic effect for the prevention of anastomotic leak. Our in vivo data herein showed that the local application of the suspension combining PF127 and EVs resulted in better healing of the colonic anastomoses compared to the control group. This difference was pre-clinically observed via a more favorable endoscopic score and a lower intensity of intraperitoneal adhesions and inflammation. This therapeutic effect was evidenced in histology by a smaller ulcerated area, less fibrous and inflammatory infiltrate of the anastomosis in the group treated with gel-embedded EVs than in the control group.

The results developed in this study are close to those obtained by our team on a similar model using ADSCs alone[14,37]. In a first study, we showed that MSCs had a therapeutic effect on high-risk colonic anastomoses by allowing a better local vascularization and a decrease in inflammation[14]. In the continuation of this work, it was shown that the administration of MSCs in a hydrogel allowed for easier administration at the anastomosis level as well as a progressive diffusion[37]. The in vivo experimental model used in this present study was adapted. Unlike the two previous studies, we performed a fractionated colorectal irradiation. We decided to perform a fractionated irradiation of 3 × 12.5 Gy focused on the colorectal area. Dose fractionation allowed us to reduce toxicity and to come closer to the clinical protocols of radiotherapy. In addition, the Biologically Effective Dose (BED) of this irradiation was 84.38 Gy, which is close to the BED observed in rectal cancer irradiation[49].

This irradiation, more similar to what is performed in clinical practice, allowed us to perform the digestive anastomosis in irradiated tissue. One of the strengths of our study is the multimodal evaluation of the clinical effectiveness of EVs on this high-risk anastomosis. The application of EVs in the gel resulted in improved endoscopic healing at the anastomosis level. However, the healing was not complete at the time of the evaluation. A future perspective would be to repeat the administration of EVs in the gel at the anastomosis level, for example

endoscopically. Interestingly, the autopsy performed showed less peri-anastomotic inflammation in the EVs + gel group with a low Zuhlke score and less adhesion at the anastomosis level. Post-operative adhesions and peri-anastomotic inflammation are a common complication in gastro-intestinal surgery[50]. The use of EVs embedded in the PF-127 gel in this preclinical study did not appear to increase this risk.

This investigation can be considered as a first step in the perspective to reach the clinical investigation of ADSC EVs for the prevention of anastomotic leaks. Although the production of EVs via a method enabling high yield and scalability was considered herein, several issues remain to be addressed, such as the design of a consolidated quality control strategy and the investigation of the optimal dose, mechanism of action as well as the long-term safety. All these issues remain an exciting challenge for future studies.

Methods

ADSC culture and characterization

Subcutaneous inguinal adipose tissue was removed from green-fluorescent-protein Sprague Dawley (SD) rats, finely minced, and enzymatically digested at 37 °C in minimum essential media (MEM) containing 0.1% collagenase type I (Sigma-Aldrich) for 30 min, 3 times. The digested tissue was filtered through a 100 µm filter. Collagenase was then neutralized with culture medium containing 10% fetal bovine serum (FBS). After centrifugation (1200 rpm for 3 min), cells were suspended in MEMα containing 20% FBS, penicillin– streptomycin and L-glutamin (all from Invitrogen) plated at 1000 cells by cm^2 and cultured at 37 °C in humidified 5% CO_2. The phenotype of amplified ADSC was verified by flow cytometry. The percentage of CD90 (clone OX-7; BD Biosciences) and CD73 (clone 5 F/B9; BD Biosciences) positive cells were analyzed, and the absence of hematopoietic cells was verified with CD34 (clone ICO115, Santa Cruz Biotechnology) and CD45 (clone OX-1; BD Biosciences) markers. Isotype identical antibodies served as controls.

EVs production

Microcarriers of 200 µm (Cytodex 1, GE Healthcare) were diluted in Phosphate Buffered Saline (PBS) and sterilized using an autoclave. PBS was then replaced by MEMα and stored at 4 °C. Before seeding the cells, microcarriers were incubated in 37 °C complete MEMα (Dulbecco) at a 19 g/L concentration during 3 h. Cells were seeded with a cell to microcarrier ratio of 20/1 and submitted to 24 cycles of 45 min of rest followed by 3 min of a gentle mixing at 60 revolutions per minute (RPM) in 1 L bioreactor. After cell adhesion, bioreactor was supplemented with complete MEMα (Dulbecco) and incubated at 37 °C and 60 RPM until confluence. Every 2 days 50% of the medium was changed. Once cells were confluent on microcarriers, turbulence triggered EV production was launched. Cells on microcarriers were washed 5 times with serum-free MEMα (Dulbecco). EV production was carried out as previously described[30]. In brief, the spinner flask bioreactor containing a magnetized paddle was placed on a magnetic stirrer to obtain a smaller vortex diameter of 35 µm (Kolmogorov length) for 4 h to generate a shear stress allowing high yield production of EVs. After that, cellular debris of the supernatant were removed by centrifugation at 2000 × *g* for 10 min. The supernatant solution was then ultra-centrifuged at 150,000 × *g* for 1.5 h to obtain an EV pellet.

EV characterization

Suspensions containing EVs were analyzed using a NanoSight LM10-HS (NanoSight, UK) with a 405 nm laser or a NS300 (NanoSight, UK). A total of 10 videos of 30 s duration were recorded, and EVs Brownian movement was tracked by nanoparticle tracking analysis (NTA) software in a frame-to-frame basis. The two-dimensional Stokes—Einstein equation was used to compute particle size from the velocity of EVs movement. The optimization of NTA post-acquisition settings was performed and these parameters were kept constant for replicate analysis. EVs size distribution, concentration, mean, and mode were obtained.

Nano-flow cytometry

Nano-flow cytometry analysis was performed utilizing the Flow NanoAnalyzer (NanoFCM Co., LTD) in accordance with the manufacturer's guidelines. To calibrate the system, a concentration standard (200 nm PS QC beads, NanoFCM) was employed for measuring particle concentration, while a cocktail of silica beads (S16M-Exo, NanoFCM) was utilized to construct a calibration curve, facilitating the conversion of side scatter intensities to particle size. The laser configuration involved a 488 nm and 640 nm laser at 20 mW, 10% ss decay, with lens filters set at 525/40 and 670/30. The antibodies for staining were Alexa Fluor® 647-conjugated monoclonal mouse antibodies directed against CD63 (clone MX49.129.5, sc-5275 af647, Santa Cruz Biotechnology) and/or anti-CD9 (clone C-4, sc-13118 af647, Santa Cruz Biotechnology) and/or anti-CD81 (clone 5A6, sc-23962 af647, Santa Cruz Biotechnology) antibodies or isotype control (sc-516609, Santa Cruz Biotechnology). The staining process was carried out overnight at 4 °C and isotype control antibodies were utilized at identical concentrations and incubation times. Labeled vesicles were then resuspended in 50 µL of PBS and diluted 1:200 times. Positivity was defined using buffer alone (PBS), unstained vesicles, isotype controls, and auto-thresholding. Prior to staining, samples were initially acquired to determine particle concentration and were subsequently diluted for optimal staining of EVs to a concentration of 5.10^9 particles/mL. Fluorochrome-conjugated antibodies were prepared for use by centrifuging at 10,000 × *g* for 15 min or filtering through a 0.22 µm syringe filter, and were diluted 10 folds for incubation with EVs. Before measurement, the samples underwent an additional 100-fold dilution in PBS. Blank controls included PBS and antibodies diluted 1000-fold in PBS. To establish the threshold between positive events and background noise in the fluorescence channel, signals from both unstained Extracellular Vesicles (EVs) and EVs incubated with the isotype control were considered. Each measurement was conducted in triplicate to ensure accuracy. The acquired data were processed using the NF Profession 1.0 software.

TEM

EV preparations for TEM samples were submitted to negative staining protocol. In brief, 4 µL EVs either suspended in PBS or combined with 20% PF-127 were incubated on copper grids F/C (300 mesh) at room temperature for 5 min. The excess was removed with a filter paper then the samples were stained with 1% uranyl acetate for 15 s at room temperature. After removal of excess uranyl acetate, the samples were dried and analyzed using a Hitachi HT 7700 120 kV transmission electron microscope.

Pluronic ®F127 preparation

PF-127 (Sigma-Aldrich) was dissolved in sterile PBS at a 20% concentration and stirred at 4 °C for 24 h. After solubilization, it was filtered with a 0.2 µm filter at 4 °C. A tube reversal test was applied to assess the solubilization at 4 °C and the viscosity at 27 °C.

Preparation of Pluronic ®F127 containing EVs (gel + EVs) and EVs alone for local administration

PF-127 (Sigma-Aldrich) was dissolved in sterile PBS at a 25% concentration and stirred at 4 °C for 24 h. After solubilization, it was filtered with a 0.2 µm filter at 4 °C. A tube reversal test was applied at 4 °C and at 27°Cto assess the thermoresponsiveness. Then ADSC EVs suspended in PBS were added to the gel, whose final concentration was 20% PF-127 and 1.10^{11} EVs/mL.

On the day of surgery, ADSC EVs were dissolved in sterile PBS at 4 °C. The final concentration was 1.10^{11}EVs/mL.

In vitro assessment of EV pro-angiogenic properties by HUVEC scratch test

Human Umbilical Vein Endothelial Cells (HUVEC) were cultured at 37 °C and 5% CO_2, using complete Endothelial Cell Growth Medium (EGM). Cells were cultured in 175 cm^2 flasks until confluence. Pro-angiogenic properties of EVs were tested using a scratch test. Monolayers of confluent HUVEC cells in 96-well plates were scratched using 96-Well WoundMaker

(Essenbioscience) and the medium was replaced to discard detached cells. HUVEC scratched monolayers were incubated for 24 h in IncuCyte live cell imager (Essenbioscience) with serum-free EGM medium. We tested increasing doses of EVs (5.10^9 to 1.10^6 EVs/mL) on the one hand and increasing doses of gel-encapsulated EVs (1.10^9 to 1.10^6 EVs/mL) on the other hand. Complete medium and serum-free medium were used as positive and negative controls respectively in the EVs alone experiment. Complete medium and PF-127 alone were used as positive and negative controls respectively in the EVs + PF-127 experiment. The percentage of migration was assessed via the gap width between wound edges measured using IncuCyte software (Essenbioscience) at 6, 12, and 18 h time points.

In vitro assessment of EV immunomodulatory properties by MLR

Lymphocytes were isolated from the thymus of SD/CD and Wistar strain rats. Lymphocytes from both strains were mixed in culture medium at a 1:1 ratio in 96 U-bottom well plates (5.10^5 per well in triplicate) and stimulated with PHA-M (Gibco®) at 1% and ConA (Sigma) at 5 µg/ml during 48 h. The cells were then treated for 24 h with rat ADSC EVs suspended in PBS at doses of 0 (negative control), $8.7.10^9$, $1.7.10^{10}$, $3.5.10^{10}$, or $7.0.10^{10}$ particles per well. ADSCs (0,5 million per well) were used as a positive control. Lymphocyte proliferation was quantified using the commercial assay Kit Roche Diagnostic ELISA BrdU (#11 647 229 001) according to the manufacturer's instructions. In brief, the cells were incubated with BrdU (1/100). After washing, fixation, and denaturation steps, intercalated BrdU was revealed by anti-BrdU antiboby, then TMB substrate. After adding stop solution, the ELISA plate was read by spectrophotometer at 450 nm.

Experimental protocol overview

All experiments were performed at the animal facilities of the Institut de Radioprotection et de Sûreté Nucléaire (Fontenay-aux-Roses, France, registry n°C92-032-01) in strict compliance with European directives (86/609/CEE) and were approved by local ethical committee of the Institute of Radioprotection and Nuclear Safety in Fontenay-aux-Roses. The experimental protocol was submitted to the French national authorization platform and after approval was registered under the APAFiS permit number #14843-201804241155405 v2 P18-03. We have complied with all relevant ethical regulations for animal use.

Forty SD rats (7 weeks-old male rats of 250 to 300, Janvier-labs, France) were randomized into 4 groups of 10 rats. They were housed in a temperature-controlled room (21 ± 1 °C) and were exposed to a 12-h light/dark cycle and fed with standard pellets with food and water available ad libitum. After an acclimatization period of a week, each rat received a fractioned irradiation of 3 × 12.5 Gray (Gy) in 1 week. Surgery was performed 3 weeks later with a low colo-colonic anastomosis during which the treatment of interest was applied (control, PF-127 alone, EVs alone or PF-127 containing EVs). Eight weeks after the end of the irradiation, colo-colic anastomoses were evaluated by colonoscopy. Immediately after colonoscopy, the rats were sacrificed and an autopsy was performed. The colonic anastomosis was then extracted for histological analysis (Fig. 1). The physical condition of the rats was monitored on a daily basis. In case of reaching the ethical limit points defined in the protocol, the rats were euthanized under general anesthesia and an autopsy was performed.

Irradiation protocol

Rats submitted to radiotherapy were anesthetized by isoflurane inhalation, and a 12.5 Gy dose was delivered three times in 1 week through a 2×3 cm window centered on the colorectal region using a medical accelerator (Elekta synergy_4MVp X-rays with a mean photon energy of about 1.5 MeV; 30 kA).

Surgery protocol and treatment procedures

3 weeks after the colorectal irradiation, colonic surgery was performed under general anesthesia by isoflurane inhalation (induction 5%, maintenance 3% in ambient air at 0.4 L/min) and prior analgesia with buprenorphine 0.5 mg/kg. All surgeries were performed by a single experimenter. The rat was maintained in a dorsal decubitus position under sterile condition on a heated operation table. The abdomen of the rat was shaved just before surgery and disinfected with povidone-iodine. A 3 cm low median laparotomy was performed. The regions of interest were the distal colon and the rectum with the hip as the lower limit and the middle colonic artery as the upper limit. The cecum and the small bowel were protected and kept out of the surgical field. The abdominal wall was exposed with two monocryl 4/0 traction points (Ethicon, France). A 5 mm portion of colon in the center of the irradiated area, ~4 cm from the anus, was resected using dissecting scissors. After an initial anchor point was made with 6/0 PDS (Ethicon, France), the anti-mesocolic side was sutured with separate 6/0 PDS stitches every 2 mm. After rotating the colon clockwise to expose the mesocolic portion of the anastomosis, the treatment was administrated. Thus, rats in the control group were injected at the upper and lower poles of the anastomosis with 50 µL of PBS and received an enema with 100 µL of PBS at the upper and lower poles of the anastomosis. Rats in the PF-127 group were injected with 50 µL of PBS at the upper and lower poles of the anastomosis and received an enema with 100 µL of PF-127 covering both the upper and lower poles of the anastomosis. Rats in the EVs group were injected at the upper and lower poles of the anastomosis with 50 µL of EVs each for a total dose of 1.10^{10} EVs, and received an enema with 100 µL of EVs for a total dose of 1.10^{10} EVs covering both the upper and lower poles of the anastomosis. Rats in the PF-127 containing EVs group received an injection of 50 µL of EVs in PBS at the upper and lower poles of the anastomosis for a total dose of 1.10^{10} EVs, and an enema of 100 µL of EVs embedded in PF-127 for a total dose of 1.10^{10} EVs covering both the upper and lower poles of the anastomosis. The injections were performed with a 25 G needle and the application of the substance of interest by enema using a flexible feeding tube. Then, the mesocolic part of the anastomosis was sutured. The abdominal cavity was then washed with warm saline and closed with a 3/0 vicryl suture (Ethicon, France). The skin portion of the incision was closed with 6 to 7 surgical staples (5.7 × 3.9 mm).

Postoperatively, the rats were evaluated daily for physical and behavioral performance. A subcutaneous injection of 0.25 mg/kg buprenorphine was performed 4–6 h after surgery and the following morning. Upon awakening, the rats were provided with food and water ad libitum. The staples were removed 15 days after surgery during a short general anesthesia with 2% isoflurane.

Colonoscopy protocol

Eight weeks after colorectal irradiation, a colonoscopy was performed to evaluate the anastomosis healing. Under general anesthesia with 2% isoflurane, rats were placed in dorsal decubitus on a heated operation table. A COLOVIEW murine endoscopy system (Karl Storz, Germany) was used. The colon was dilated during the examination by continuous injection of saline through the operating channel using a 20 mL syringe. The anastomosis was located ~4 cm from the anal margin. The feces were washed out with saline injected through the working channel and by abdominal mobilization. The anastomosis was filmed and pictures were taken. The images were then read by an experienced gastro-enterologist blinded to the treatment received by the specimens. The presence of anastomotic ulceration and its characterization was scored according to its severity (1: no ulcer, 2: superficial ulcer, 3: deep ulcer, 4: deep circumferential ulcer)[14]. Bleeding or stenosis of the anastomosis was also reported. An endoscopic inflammation score from 1 to 6 (ENDOSCORE) was then calculated by adding the grade of the ulcer (1-4), the presence or absence of bleeding (0-1), the presence or absence of anastomotic stricture (0-1).

Autopsy protocol

Immediately after colonoscopy, the rats were killed by cardiac puncture under 2% isoflurane anesthesia, and an autopsy was performed. The occurrence of intra-abdominal leak, peritoneal adhesion, and the number of structures adherent to the anastomosis (seminal vesicles, bladder, small bowel) was investigated before performing a total colectomy removing the anastomosis. Peritoneal adhesions were assessed by the Zuhlke score,

commonly used in preclinical studies[51]. The colonic specimen was then centered on the anastomosis, washed with saline, embedded in a cassette, and placed in 4% formaldehyde. The autopsy was performed by a digestive surgeon blinded to the treatment received by the rats.

Histological analysis and fibrosis quantification

After 24 h in 4% formaldehyde, the colon blocks were embedded in paraffin after preparation with Tissue-Tek VIP6 (Sekura, France). The embedded colon blocks were then cut with a rotary microtome (Leica, Germany) into 5 sets of 10 slides of 5 µm thickness. The series were spaced 150 µm apart. One slide from each series was stained with Hematoxylin-Eosin-Safran (HES), Masson's Trichrome (TM) and Sirius Red (SR). The slides were then scanned at 20× magnification using a slide scanner Lamina (Perkin Elmer, USA). The slides were read by a single experimenter blinded to the treatment received by the rats using CaseViewer software (3DHISTECH, Hungary).

The mean size of the ulcerated area (epithelial denudation) were reported after reading the HES.

Using the FIBER-ML program developed from MATLAB by our team, we quantified collagen at the anastomotic level by machine-learning[52]. The SR stained slides were selected and centered on the anastomosis and exported at ×100 magnification in TIFF format. After manual reading of 5 slides and by delimiting the collagenous zones (red), matrix zones (yellow) and the background (gray), we launched the program to analyze all the selected slides. The collagen surface per slide was calculated. We then performed a quality control on 25% of the sample.

Immunohistochemistry

For PMN detection by immunohistochemistry, sections were dewaxed and then placed in antigen retrieval solution (0.01 M citrate buffer, pH = 6 (DakoCytomation, France) for 3 × 5 min at 350 W). Endogenous peroxidases were inhibited by incubation with 3% H_2O_2 in methanol at room temperature for 10 min. After saturation (X0909; DakoCytomation), 35-fold diluted rabbit anti-rat MPO (Abcam, France) was applied to the slide for 1 h at 37 °C. Staining was developed with Histo-Green substrate (E109; Abcys), and the slides were counterstained with Fast Nuclear Red (S1963; DakoCytomation, France), dehydrated and mounted. Isotype controls were used as negative controls. The number of neutrophils (MPO positive) at the anastomosis was reported for a defined area.

For CD68 immunostaining (macrophage analysis), tissue sections were treated with proteinase K (DakoCytomation) at room temperature and quenched for endogenous peroxidases described above. After saturation, 200-fold diluted mouse antirat CD68 (AbD Serotec) was applied to the section for 1 h at 37 °C. Staining was developed with Histo-Green substrate (E109; Abcys), and the slides were counterstained with Fast Nuclear Red (S1963; DakoCytomation, France), dehydrated and mounted. Isotype controls were used as negative controls. The number of macrophages (CD68 positive) at the anastomosis was reported for a defined area.

Statistics and reproducibility

Normal continuous variables were described by their means and standard deviations. Non-normal continuous variables were described by their medians and interquartile ranges (Q1–Q3). Categorical variables were described by their numbers and percentages. Fischer's exact test was carried out for comparisons between categorical variables and the nonparametric Mann–Whitney test was used for non-paired continuous variables.

Comparison between more than two-groups of non-normal quantitative variables was performed using a non-parametric Kruskall-Wallis test, if a statistical difference was found, the samples were compared in pairs by a Dwass-Steel-Crtichlow-Fligner multiple weighted test. Comparison between more than two-groups of normal quantitative variables was performed using an ANOVA, if a statistical difference was found, the samples were compared in pairs by a Tukey multiple weighted test. All tests were two-tailed with a significance level of $p < 0.05$. All analyses were performed with R software version 3.6.0. or GraphPadPrism (GraphPad Software, La Jolla, USA).

Reporting summary

Further information on research design is available in the Nature Portfolio Reporting Summary linked to this article.

Data availability

The numerical source data underlying the graphs shown in the figures can be found in Supplementary Data. All other data are available from the corresponding author upon reasonable request.

Received: 23 January 2023; Accepted: 4 December 2024;
Published online: 19 December 2024

References

1. Siegel, R. L., Miller, K. D. & Jemal, A. Cancer statistics, 2018: cancer statistics, 2018. *CA Cancer J. Clin.* **68**, 7–30 (2018).
2. Glynne-Jones, R., Wyrwicz, L. & Tiret, E. et al. Rectal cancer: ESMO Clinical Practice Guidelines for diagnosis, treatment and follow-up. *Ann. Oncol.* **28**, iv22–iv40 (2017).
3. Penna, M., Hompes, R. & Arnold, S. et al. Incidence and risk factors for anastomotic failure in 1594 patients treated by transanal total mesorectal excision: results from the international TaTME registry. *Ann. Surg.* **269**, 700–711 (2019).
4. Alves, A. Postoperative mortality and morbidity in French patients undergoing colorectal surgery: results of a prospective multicenter study. *Arch. Surg.* **140**, 278 (2005).
5. Krarup, P. M., Nordholm-Carstensen, A., Jorgensen, L. N. & Harling, H. Anastomotic leak increases distant recurrence and long-term mortality after curative resection for colonic cancer: a nationwide cohort study. *Ann. Surg.* **259**, 930–938 (2014).
6. Hammond, J., Lim, S., Wan, Y., Gao, X. & Patkar, A. The burden of gastrointestinal anastomotic leaks: an evaluation of clinical and economic outcomes. *J. Gastrointest. Surg.* **18**, 1176–1185 (2014).
7. Vallance, A., Wexner, S. & Berho, M. et al. A collaborative review of the current concepts and challenges of anastomotic leaks in colorectal surgery. *Colorectal Dis.* **19**, O1–O12 (2017).
8. Kawada, K. & Sakai, Y. Preoperative, intraoperative and postoperative risk factors for anastomotic leakage after laparoscopic low anterior resection with double stapling technique anastomosis. *World J. Gastroenterol.* **22**, 5718 (2016).
9. Sparreboom, C. L., Wu, Z. & Lingsma, H. F. et al. Anastomotic leakage and interval between preoperative short-course radiotherapy and operation for rectal cancer. *J. Am. Coll. Surg.* **227**, 223–231 (2018).
10. Foppa, C., Ng, S. C., Montorsi, M. & Spinelli, A. Anastomotic leak in colorectal cancer patients: new insights and perspectives. *Eur. J. Surg. Oncol.* **46**, 943–954 (2020).
11. Degiuli, M., Elmore, U. & De Luca, R. et al. Risk factors for anastomotic leakage after anterior resection for rectal cancer (RALAR study): A nationwide retrospective study of the Italian Society of Surgical Oncology Colorectal Cancer Network Collaborative Group. *Colorectal Dis.* **24**, 264–276 (2022).
12. Ma, B., Gao, P. & Wang, H. et al. What has preoperative radio(chemo) therapy brought to localized rectal cancer patients in terms of perioperative and long-term outcomes over the past decades? A systematic review and meta-analysis based on 41,121 patients: PRT/PCRT-Perioperative and long-term outcomes over the past decades. *Int. J. Cancer* **141**, 1052–1065 (2017).
13. Lim, S. B. et al. Late anastomotic leakage after low anterior resection in rectal cancer patients: clinical characteristics and predisposing factors. *Colorectal Dis.* **18**, O135–O140 (2016).
14. Van de putte, D. et al. Adipose-derived mesenchymal stromal cells improve the healing of colonic anastomoses following high dose of

irradiation through anti-inflammatory and angiogenic processes. *Cell Transpl.* **26**, 1919–1930 (2017).
15. Maruya, Y. et al. Autologous adipose-derived stem cell sheets enhance the strength of intestinal anastomosis. *Regen. Ther.* **7**, 24–33 (2017).
16. Sukho, P. et al. Effects of adipose stem cell sheets on colon anastomotic leakage in an experimental model: Proof of principle. *Biomaterials* **140**, 69–78 (2017).
17. Alvarenga, V. et al. Protective effect of adipose tissue–derived mesenchymal stromal cells in an experimental model of high-risk colonic anastomosis. *Surgery* **166**, 914–925 (2019).
18. Sémont A. et al. Mesenchymal stem cell therapy stimulates endogenous host progenitor cells to improve colonic epithelial regeneration. *PLoS ONE* **8**, e70170. https://doi.org/10.1371/journal.pone.0070170 (2013).
19. Lai, R. C., Chen, T. S. & Lim, S. K. Mesenchymal stem cell exosome: a novel stem cell-based therapy for cardiovascular disease. *Regen. Med.* **6**, 481–492 (2011).
20. Lai, R. C., Yeo, R. W. Y. & Lim, S. K. Mesenchymal stem cell exosomes. *Semin. Cell Dev. Biol.* **40**, 82–88 (2015).
21. Zaborowski, M. P., Balaj, L., Breakefield, X. O. & Lai, C. P. Extracellular vesicles: composition, biological relevance, and methods of study. *BioScience* **65**, 783–797 (2015).
22. Yáñez-Mó, M., Siljander, P. R. M. & Andreu, Z. et al. Biological properties of extracellular vesicles and their physiological functions. *J. Extracell. Vesicles* **4**, 27066 (2015).
23. EL Andaloussi, S., Mäger, I., Breakefield, X. O. & Wood, M. J. A. Extracellular vesicles: biology and emerging therapeutic opportunities. *Nat. Rev. Drug Discov.* **12**, 347–357 (2013).
24. Bruno, S. et al. Microvesicles derived from mesenchymal stem cells enhance survival in a lethal model of acute kidney injury. *PLoS ONE* **7**, e33115. https://doi.org/10.1371/journal.pone.0033115 (2012).
25. Lai, R. C. et al. Exosome secreted by MSC reduces myocardial ischemia/reperfusion injury. *Stem Cell Res.* **4**, 214–222 (2010).
26. Li, T. et al. Exosomes derived from human umbilical cord mesenchymal stem cells alleviate liver fibrosis. *Stem Cells Dev.* **22**, 845–854 (2013).
27. Zhang, B. et al. HucMSC-exosome mediated-wnt4 signaling is required for cutaneous wound healing: HucMSC-exosome enhances cutaneous wound healing. *Stem Cells* **33**, 2158–2168 (2015).
28. Long, Q. et al. Intranasal MSC-derived A1-exosomes ease inflammation, and prevent abnormal neurogenesis and memory dysfunction after status epilepticus. *Proc. Natl. Acad. Sci. USA* **114**, E3536–E3545 (2017).
29. Vader, P., Mol, E. A., Pasterkamp, G. & Schiffelers, R. M. Extracellular vesicles for drug delivery. *Adv. Drug Deliv. Rev.* **106**, 148–156 (2016).
30. György, B., Hung, M. E., Breakefield, X. O. & Leonard, J. N. Therapeutic applications of extracellular vesicles: clinical promise and open questions. *Annu. Rev. Pharm. Toxicol.* **55**, 439–464 (2015).
31. Klouda, L. Thermoresponsive hydrogels in biomedical applications. *Eur. J. Pharm. Biopharm.* **97**, 338–349 (2015).
32. Silva, A. K. A. et al. Thermoresponsive gel embedded with adipose stem-cell-derived extracellular vesicles promotes esophageal fistula healing in a thermo-actuated delivery strategy. *ACS Nano* **12**, 9800–9814 (2018).
33. Berger, A. et al. Local administration of stem cell-derived extracellular vesicles in a thermoresponsive hydrogel promotes a pro-healing effect in a rat model of colo-cutaneous post-surgical fistula. *Nanoscale* **13**, 218–232 (2021).
34. Cong, Z. et al. Influencing factors of symptomatic anastomotic leakage after anterior resection of the rectum for cancer. *World J. Surg.* **33**, 1292–1297 (2009).
35. Stumpf, M. et al. Changes of the extracellular matrix as a risk factor for anastomotic leakage after large bowel surgery. *Surgery* **137**, 229–234 (2005).
36. Karliczek, A. et al. Intraoperative assessment of microperfusion with visible light spectroscopy for prediction of anastomotic leakage in colorectal anastomoses: VLS in anastomotic leakage prediction. *Colorectal Dis.* **12**, 1018–1025 (2010).
37. Moussa, L. et al. Heparan sulfate mimetics: a new way to optimize therapeutic effects of hydrogel-embedded mesenchymal stromal cells in colonic radiation-induced damage. *Sci. Rep.* **9**. https://doi.org/10.1038/s41598-018-36631-6 (2019).
38. Rani, S., Ryan, A. E., Griffin, M. D. & Ritter, T. Mesenchymal stem cell-derived extracellular vesicles: toward cell-free therapeutic applications. *Mol. Ther.* **23**, 812–823 (2015).
39. Piffoux M. et al. Extracellular vesicles for personalized medicine: the input of physically triggered production, loading and theranostic properties. *Adv. Drug Deliv. Rev*. Published online December 2018. https://doi.org/10.1016/j.addr.2018.12.009 (2019).
40. Gazeau, F., Silva, A. K. A., Merten, O. W., Wilhelm, C., & Piffoux, M. Fluid system for producing extracellular vesicles and associated method. US patent WO/2019/002608 (2019).
41. Coffin, E. et al. Extracellular vesicles from adipose stromal cells combined with a thermoresponsive hydrogel prevent esophageal stricture after extensive endoscopic submucosal dissection in a porcine model. *Nanoscale* **13**, 14866–14878 (2021).
42. Batrakova, E. V. & Kabanov, A. V. Pluronic block copolymers: evolution of drug delivery concept from inert nanocarriers to biological response modifiers. *J. Control. Release* **130**, 98–106 (2008).
43. An, J. H., Li, Q., Bhang, D. H., Song, W. J. & Youn, H. Y. TNF-α and INF-γ primed canine stem cell-derived extracellular vesicles alleviate experimental murine colitis. *Sci. Rep.* **10**, 2115 (2020).
44. Cheng, A. et al. Human multipotent mesenchymal stromal cells cytokine priming promotes RAB27B-regulated secretion of small extracellular vesicles with immunomodulatory cargo. *Stem Cell Res. Ther.* **11**, 539 (2020).
45. Rozier, P. et al. Lung fibrosis is improved by extracellular vesicles from IFNγ-primed mesenchymal stromal cells in murine systemic sclerosis. *Cells* **10**, 2727 (2021).
46. Warnecke, A. et al. Extracellular vesicles from human multipotent stromal cells protect against hearing loss after noise trauma in vivo. *Clin. Transl. Med.* **10**, e262 (2020).
47. Gorgun, C. et al. Role of extracellular vesicles from adipose tissue- and bone marrow-mesenchymal stromal cells in endothelial proliferation and chondrogenesis. *Stem Cells Transl. Med.* **10**, 1680–1695 (2021).
48. Gregorius, J. et al. Small extracellular vesicles obtained from hypoxic mesenchymal stromal cells have unique characteristics that promote cerebral angiogenesis, brain remodeling and neurological recovery after focal cerebral ischemia in mice. *Basic Res. Cardiol.* **116**, 40 (2021).
49. Beskow, C., Ågren-Cronqvist, A. K., Lewensohn, R. & Toma-Dasu, I. Biological effective dose evaluation and assessment of rectal and bladder complications for cervical cancer treated with radiotherapy and surgery. *J. Contemp. Brachytherapy* **4**, 205–212 (2012).
50. van Goor, H. Consequences and complications of peritoneal adhesions. *Colorectal Dis.* **9**, 25–34 (2007).
51. Zühlke, H. V., Lorenz, E. M., Straub, E. M. & Savvas, V. Pathophysiology and classification of adhesions. *Langenbecks Arch. Chir. Suppl. II Verh. Dtsch. Ges. Chir*. 1009–1016 (1990).
52. Facchin, C. et al. FIBER-ML, an open-source supervised machine learning tool for quantification of fibrosis in tissue sections. *Am. J. Pathol.* **192**, 783–793 (2022).

Acknowledgements

This work was supported by the IdEx Université Paris Cité, ANR-18-IDEX-0001 (IVETh plateform), by the Region Ile de France under the convention SESAME 2019—IVETh (EX047011) (IVETh plateform) and by the Region Ile de France and Banque pour l'Investissement (BPI) under the convention

Accompagnement et transformation des filières projet de recherché et développement N° DOS0154423/00 & DOS0154424/00 (IVETh platform). This project has received funding from CNRS, from the European Research Council (ERC) under the European Union's Horizon 2020 research and innovation program (grant agreement No. 852791) and from Fondation ARC.

Author contributions

Guarantor of article: G.R. Conception and design of the study: H.A., N.M., A.S., G.R. Generation, collection, assembly, analysis and/or interpretation of data: H.A., N.M., G.P., A.C.S., C.D., A.C., I.A.F., A.S., G.R. Drafting or revision of the manuscript: H.A., N.M., G.P., A.C.S., C.D., A.C., A.B., B.M., C.W., F.G., A.M., M.K., O.C., I.A.F., A.S., G.R. Approval of the final version of the manuscript: H.A., N.M., G.P., A.C.S., C.D., A.C., A.B., B.M., C.W., F.G., A.M., M.K., O.C., I.A.F., A.S., G.R.

Competing interests

H.A., N.M., G.P., A.C.S., C.D., A.C., A.B., B.M., A.M., O.C., I.A.F. declare no competing interest. G.R. received personal fees from FUJIFILM, MEDTRONIC, and grants from NORGINE. F.G., A.S., C.W., and G.R. are co-founders of the spin-off Evora Biosciences. A.S. and C.W. are co-founders of the spin-off EverZom.

Additional information

Supplementary information The online version contains supplementary material available at https://doi.org/10.1038/s42003-024-07364-2.

Correspondence and requests for materials should be addressed to Hadrien Alric.

Peer review information *Communications Biology* thanks the anonymous, reviewer(s) for their contribution to the peer review of this work. Primary Handling Editors: Georgios Giamas, Anam Akhtar, and Dario Ummarino.